Electronic structure of $CeCuAs_2$

A. Chainani,[1,2,*] M. Matsunami,[3] M. Taguchi,[3] R. Eguchi,[4] Y. Takata,[1,†] M. Oura,[5] S. Shin,[3,6] K. Sengupta,[7] E. V. Sampathkumaran,[7] Th. Doert,[8] Y. Senba,[9] H. Ohashi,[9] K. Tamasaku,[1] Y. Kohmura,[1] M. Yabashi,[1] and T. Ishikawa[1]

[1]*Coherent X-ray Optics Laboratory, RIKEN SPring-8 Center, 1-1-1 Sayo-cho, Hyogo 679-5148, Japan*
[2]*Department of Physics, Tohoku University, Aramaki, Aoba-ku, Sendai 980 8578, Japan*
[3]*Excitation-order Research Team, RIKEN SPring-8 Center, 1-1-1 Sayo-cho, Hyogo 679-5148, Japan*
[4]*Research Laboratory for Surface Science, Okayama University, Okayama 700-8530, Japan*
[5]*Advanced Photon Technology Division, RIKEN SPring-8 Center, 1-1-1 Sayo-cho, Hyogo 679-5148, Japan*
[6]*Institute for Solid State Physics, The University of Tokyo, Kashiwa, Chiba 277-8581, Japan*
[7]*Tata Institute of Fundamental Research, Homi Bhabha Road, Mumbai 400-005, India*
[8]*Technische Universitat Dresden, Department of Chemistry and Food Chemistry, D-01062 Dresden, Germany*
[9]*JASRI/SPring-8, Sayo-cho, Hyogo 679-5148, Japan*

(Received 5 September 2013; revised manuscript received 9 April 2014; published 17 June 2014)

We study the electronic structure of $CeCuAs_2$, which is known to show an anomalous negative temperature coefficient of resistivity below room temperature, while the thermopower shows metallic behavior. We carry out hard x-ray photoemission spectroscopy (PES), x-ray absorption spectroscopy (XAS), and resonant PES across the Ce $3d$-$4f$ and Cu $2p$-$3d$ thresholds to investigate the role of Kondo screening in $CeCuAs_2$. The Ce $3d$ core-level PES shows the f^0, f^1, and f^2 features, and the Ce $3d$-$4f$ XAS shows corresponding features due to transitions into the f^1 and f^2 states, as in Kondo systems. The spectral feature assignments are confirmed by single-impurity Anderson model calculations and indicate a nearly trivalent-Ce configuration with small but finite mixed valency. The resonant PES valence band spectra across the Ce $3d$-$4f$ threshold show an intense Ce $4f^1$ resonance just below the Fermi level, while the Ce $4f^0$ feature is observed at a binding energy of 2.5 eV. The obtained f partial density of states shows an unusual pseudogaplike dip at the Fermi level in $CeCuAs_2$. The results indicate the importance of Kondo screening and a pseudogap in the f partial density of states for the anomalous transport and magnetic properties of $CeCuAs_2$.

DOI: 10.1103/PhysRevB.89.235117 PACS number(s): 71.27.+a, 79.60.−i, 71.20.Eh

I. INTRODUCTION

The Kondo model, originally formulated to describe the behavior of a localized magnetic impurity interacting with the conduction band of a metallic host [1], continues to play a very important role in strongly correlated f-electron systems [2]. Starting with the Kondo effect in metallic alloys, it has been successfully used to explain a variety of phenomena such as heavy-fermion behavior [2,3], the volume collapse in f-electron systems [4], resonances in quantum dots [5] and quantum corrals [6], single-molecule Kondo effect [7], quantum phase transitions [8], etc. The close relation between Kondo effect and the Mott metal-insulator transition (usually associated with correlated d electrons) is also well recognized [9]. There have also been several studies of the Kondo model which have addressed the unusual properties of non-Fermi liquids [10–15]. In particular, Coleman and Pepin showed that an underscreened Kondo model results in deviations from a Fermi liquid behavior in the specific heat, which originates in an anomalous scattering of conduction electrons by the unscreened spins [12]. Florens then showed that the spectroscopic properties of the underscreened Kondo model would give a pseudogap in the density of states and a power law in transport properties [13]. It was suggested that the transport properties of the Ce compound $CeCuAs_2$ [16] seemed quite consistent with the theoretical prediction.

More recently, Nevidomskyy and Coleman have addressed the general issue of the role of Hund's coupling on the Kondo effect for d- and f-electron systems [17]. It was shown that for a single-site multi(K)-channel Kondo model with Hund coupling, underscreening results in a locking of the localized spin-$\frac{1}{2}$ moments to form a large pseudospin $S = K/2$ and the effective Kondo temperature gets reduced exponentially. This behavior can be suitably identified from a plot of $T\chi(T)$ versus $\ln T$ [where $\chi(T)$ is the magnetic susceptibility measured as a function of the temperature T], as it is expected to show an enhanced moment due to the unscreened spin $S = K/2$ at temperatures above the effective Kondo temperature (T_K^*). As discussed by the authors, this is very similar to the early theoretical prediction of Jayaprakash, Krishnamurthy, and Wilkins for the two-impurity two-channel Kondo model [18]. It was shown that for a ferromagnetic Ruderman-Kittel-Kasuya-Yosida (RKKY) interaction between the two spin-$\frac{1}{2}$ impurities, the two impurities would lock into an effective spin-1 triplet state. They also showed that if the RKKY interaction between the two impurities is antiferromagnetic, the two impurities would behave like a singlet and $T\chi(T)$ would reduce rapidly. The main theme of this work is as follows: Using various techniques of electron spectroscopy combined with single-impurity Anderson model calculations, we investigate the electronic structure of $CeCuAs_2$ and its relation with theoretical predictions discussed above. We also check the behavior of $T\chi(T)$ versus $\ln T$ for the case of $CeCuAs_2$ in order to test for underscreening.

$CeCuAs_2$ crystallizes in the $HfCuSi_2$-type layered tetragonal structure [19,20], where Si can be replaced with a pnictogen

*chainani@spring8.or.jp
†Deceased.

Pn(=P, As, Sb, Bi). Indeed, a large number of arsenides and antimonides with the formula $RM\mathrm{As}_2$ and $RM\mathrm{Sb}_2$ (R = rare earth, M = transition metal) are known to crystallize in this structure [21–25]. However, other than $CeCuAs_2$ [16], all the other isostructural compounds which exhibit a magnetic moment at high temperatures undergo magnetic ordering at low temperatures, with ordering temperatures typically between 2 to 15 K [21–25]. Even the uranium-based materials $UM\mathrm{Pn}_2$ show metallic behavior with magnetic ordering [20,26]. In contrast, a detailed investigation of $CeCuAs_2$ showed that the electrical transport was anomalous with a negative temperature coefficient of resistivity down to 45 mK and a power-law behavior at the lowest temperatures [$\rho(T) \propto T^{-0.6}$], while the thermopower showed typical metallic behavior [16]. Further, the high-temperature magnetic susceptibility revealed a magnetic moment of $\mu_{\mathrm{eff}} = 2.68\mu_B$, typical of a trivalent Ce ion. However, no magnetic ordering was found down to 45 mK, in spite of a relatively large value of the estimated paramagnetic Curie temperature ($\Theta_p = -47$ K). While the specific heat showed a rise below ~10 K, and an appreciably large Sommerfeld coefficient of 800 mJ/mol K^2 at 2 K, it got reduced to 425 mJ/mol K^2 at 0.5 K [16]. It was also shown that the temperature coefficient of electrical resistivity undergoes a sign change from negative to positive upon applying external pressure [27]. These results indicate that $CeCuAs_2$ is quite unlike other Ce-based Kondo or heavy-fermion systems [16].

In this work, we investigate the electronic structure of $CeCuAs_2$ using various techniques of electron spectroscopy. Using hard x-ray photoemission spectroscopy (HAXPES), we report on the Ce $3d$ core-level and valence band electronic structure of $CeCuAs_2$. We also carried our x-ray absorption and resonant PES across the Cu $2p$-$3d$ (L-edge) and Ce $3d$-$4f$ (M-edge) thresholds. The photoionization cross sections as a function of photon energy allow us to unambiguously identify the Ce $4f$, Cu $3d$, and As $4s$-$4p$ states in the valence band. In combination with single-impurity Anderson model calculations, we confirm $CeCuAs_2$ to be a nearly trivalent Ce^{3+} system which exhibits clear spectral signatures of Kondo screening in core-level PES and XAS. While the off-resonant data show a typical Fermi edge, from Ce $3d$-$4f$ resonant PES studies, we identify a pseudogaplike feature in the occupied $4f$ partial density of states with the main peak of the $4f$ character states lying just below, and not at, the Fermi level (E_F). However, an analysis of $T\chi(T)$ versus $\ln T$ rules out underscreening in $CeCuAs_2$, but is suggestive of nearest-neighbor antiferromagnetic correlations [18,28]. The overall results indicate Kondo screening and a pseudogap in the f partial density of states lead to the anomalous transport and magnetic properties of $CeCuAs_2$.

II. EXPERIMENTS

Polycrystalline samples of $CeCuAs_2$ were synthesized using stoichiometric amounts of the constituent elements (>99.9% purity), as described in earlier work [16,21]. The crystal structure and lattice constants were confirmed to be in good agreement with reported results [16,21]. HAXPES measurements were carried out at beamline BL29XU, SPring-8 using an incident photon energy of $h\nu = 7935$ eV and a spectrometer [29] equipped with a R-4000-10-kV VG-Scienta analyzer. The total-energy resolution was set to 225 meV for the HAXPES measurements. For the incident photon energy in HAXPES measurements, we use the Si(444) reflection in order to achieve a very high-energy resolution of $\Delta E/E = 4.8 \times 10^{-6}$ (i.e., ~40 meV at 7935 eV). The lowest limit of the energy range for the Si(444) reflection is determined by the Bragg angle of $\pi/2$ (backscattering), and this corresponds to an energy of 7910 eV. However, in practice, the channel cut monochromator we use is limited to an angle of ~85°, and the corresponding energy of the incident x rays is ~7935 eV (Ref. [27]). X-ray absorption spectroscopy (XAS) and resonant PES experiments were carried out at beamline BL17SU, SPring-8. The XAS measurements (total electron yield mode) and the resonant PES experiments were carried out using a spectrometer [30] equipped with a VG-Scienta 2002 analyzer and the total-energy resolution at the Ce $3d$-$4f$ threshold was 200 meV. The Fermi level and energy resolutions for the HAXPES and soft x-ray resonant PES measurements were determined from the Fermi edge of a gold film at $T = 20$ or 22 K, respectively. All the results reported here were obtained from samples fractured *in situ* and measured at $T = 20$ or 22 K, respectively, corresponding to the lowest temperature that could be achieved using a liquid-He flow type cryostat on the spectrometers.

III. RESULTS AND DISCUSSIONS

Figure 1 shows the experimental Ce $3d$ core-level spectrum (symbols) of $CeCuAs_2$ measured at $T = 20$ K by HAXPES ($h\nu = 7935$ eV). The spectrum consists of the Ce $3d_{5/2}$ and $3d_{3/2}$ states with main peaks at 884.5 and 902.5 eV binding energies. The spectrum also shows weak intensity

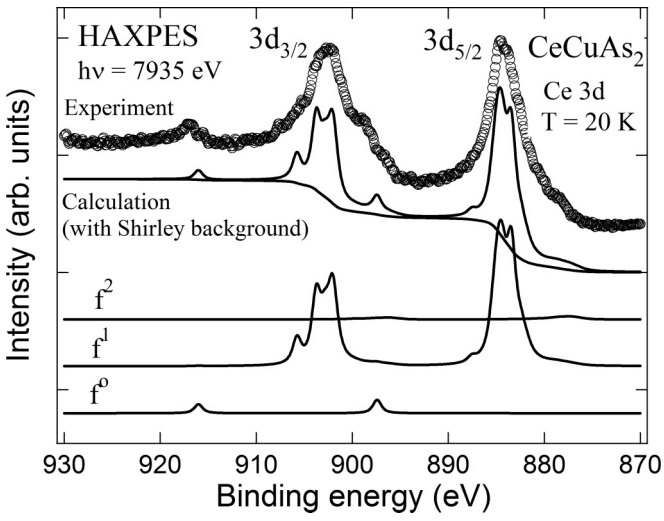

FIG. 1. The experimental Ce $3d$ core-level spectrum of $CeCuAs_2$ measured by HAXPES ($h\nu = 7935$ eV) at $T = 20$ K. The experimental spectrum is compared with the spectrum calculated using the single-impurity Anderson model, which confirms the Kondo screening derived f^0, f^1, and f^2 features of the spin-orbit split Ce $3d_{5/2}$ and $3d_{3/2}$ states. The individual f^0, f^1, and f^2 components and the Shirley background are also shown.

satellite features at higher and lower binding energies from the main peak. The main peak and weak features form a triplet and are derived from a quantum mechanical mixing of the f^0, f^1, and f^2 initial states, which essentially constitute the ground state in Kondo materials. We have carried out single-impurity Anderson model calculations which are well known to provide a consistent description of the core-level and angle-integrated valence band spectroscopic properties of Kondo systems [31–38]. The calculated Ce $3d$ core-level PES spectrum is also plotted (full lines) in Fig. 1. The calculated spectrum matches fairly with the experimental data, thereby confirming the assignments and allows a quantification of the ground state. The individual contributions of the f^0, f^1, and f^2 final states to the spectra are also shown, along with the Shirley background used to obtain a suitable match to the experiment. The calculations provide the following set of parameter values for $CeCuAs_2$: the onsite Coulomb energy $U_{ff} = 7.5$ eV, the core-hole potential $U_{fc} = 11.0$ eV, the $4f$ level energy $\epsilon_f^0 = -2.5$ eV, bandwidth $W = 3.0$ eV, and the hopping parameter between the $4f$ level and conduction band states is $V = 0.25$ eV. In terms of the conventional way [31] to describe the hybridization strength, we obtain $\Delta = 2V^2/W = 41.6$ meV. This value of Δ is close to that of the prototypical Ce^{3+} γ-Ce phase ($\Delta = 32$ meV) [35]. Another example of a nearly Ce^{3+} state with a similar value of Δ (=37 meV) is $CeNi_4Al$ [39]. The f-electron count for $CeCuAs_2$ is calculated to be $n_f = 1.01$, with the initial-state contributions of $f^0 = 1.7\%$, $f^1 = 95.8\%$, and $f^2 = 2.5\%$. These values indicate a small but finite mixed valency for $CeCuAs_2$.

Figure 2 shows a comparison of the valence band spectra obtained using HAXPES ($h\nu$= 7935 eV) at $T = 20$ K, and soft x-ray PES ($h\nu$= 922.7 eV) obtained at $T = 22$ K. Since the difference in incident photon energies results in a large change in atomic photoionization cross section (PICS) [40] of the Cu $3d$ states compared to Ce $4f$, As $4s$, and As $4p$ states, it helps in identification of the partial density of states as discussed in the following. In particular, at $h\nu$= 922.7 eV, the Cu $3d$ PICS is an order of magnitude larger than As $4s$-$4p$ and Ce $3d$ PICS, and the valence band states are expected to be dominated by Cu $3d$ states. As seen in Fig. 2, the soft x-ray PES valence band spectrum is dominated by a feature centered at about 4 eV binding energy, and of approximately 2 eV full width at half maximum (FWHM). A lower-intensity structure is seen between E_F and about 2.5 eV binding energy for the HAXPES and soft x-ray valence band spectra. In contrast, a clear feature of about 4 eV FWHM is obtained at ~11 eV binding energy in the HAXPES spectrum. This broad feature is nearly missing (the inset shows a weak bump in the ×5 magnification of the intensity scale) in the soft x-ray spectrum and is due to the As $4s$ states. This is consistent with a similar feature for As $4s$ states reported recently in $BaFe_2As_2$ using HAXPES [41]. Further, the feature at 4 eV binding energy gets broadened on the high binding energy side by about 2 eV. Given the decrease in relative atomic cross sections of the Cu $3d$ states on going to high photon energies ($h\nu = 7935$) compared to the As $4s$-$4p$ states, it is clear that the soft x-ray spectrum is dominated by the Cu $3d$ states centered at 4 eV binding energy, while the HAXPES spectrum shows dominantly As $4p$ states between 3–6 eV binding energies mixed with Cu $3d$ character states. The occupied Ce $4f$ states are strongly suppressed at soft x-ray and hard x-ray energies due to low cross sections and,

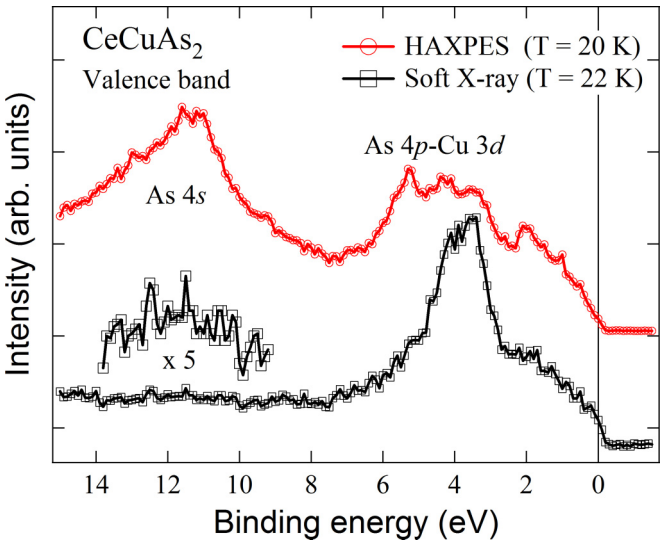

FIG. 2. (Color online) Comparison of the valence band spectra obtained using HAXPES ($h\nu = 7935$ eV) at $T = 20$ K, and soft x-ray PES ($h\nu = 922.7$ eV) obtained at $T = 22$ K.

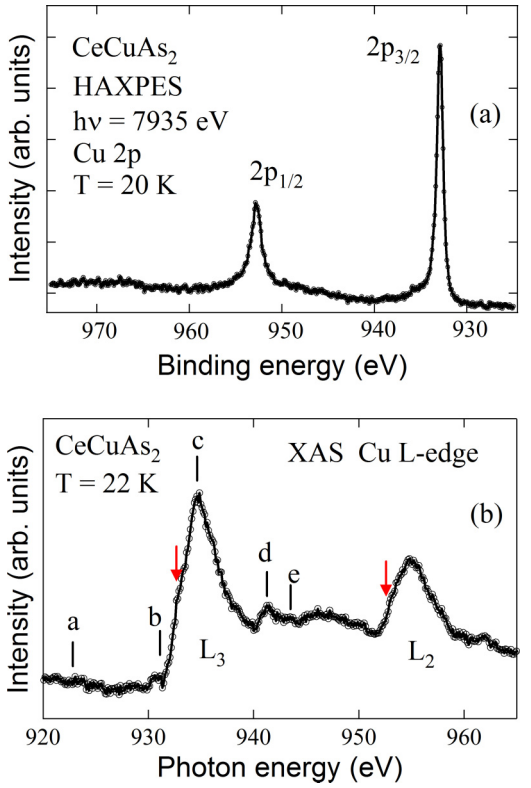

FIG. 3. (Color online) (a) The Cu $2p$ core-level HAXPES spectrum measured at $T = 20$ K indicative of a nominal Cu^{1+} valency. (b) The Cu L-edge XAS spectrum measured at $T = 22$ K. The red arrows correspond to the peak positions obtained from the HAXPES Cu $2p$ spectrum. The labels a–e correspond to the photon energies used for the Cu $2p$-$3d$ resonant photoemission spectra shown in Fig. 4.

as will be shown in the following using resonant PES, occur between E_F and 2.5-eV binding energy. Accordingly, we have carried out Cu $2p$-$3d$ and Ce $3d$-$4f$ resonant PES but, prior to that, we first discuss the Cu $2p$ core-level HAXPES and the corresponding Cu L-edge XAS spectra.

Figure 3(a) shows the HAXPES Cu $2p$ core-level spectra measured at $T = 20$ K. As is known from early work [42], the Cu $2p$ spectra can be used to fingerprint the nominal valency of the Cu states in $CeCuAs_2$. The spectrum shows clean single peaks for the $2p_{3/2}$ and the $2p_{1/2}$ features at binding energies of 932.9 and 952.7 eV. The binding energies and spectral shape, i.e., narrow single peaks for the $2p_{3/2}$ and the $2p_{1/2}$ features without satellites, indicates a nominal Cu^{1+}, although the binding energies obtained here are 0.5 eV higher than for Cu_2O [42]. The Cu^{2+} state, in contrast, is known to show a broad main peak with a satellite feature at about 9 eV higher binding energy [42], and the satellite is clearly missing in $CeCuAs_2$. Figure 3(b) shows the Cu L-edge XAS spectrum with an L_3 peak at 934.6-eV and the L_2 peak at 954.8-eV photon energies. These main peak positions are higher by about 1 eV compared to those of Cu_2O [43,44], but it is noted that the onset energies correspond well to the core-level peak positions obtained from HAXPES, as shown by red arrows in Fig. 3(b). From careful studies of the XAS of Cu, Cu_2O, and CuO, it is known that the main peak of the Cu_2O spectrum shows an excitonlike contribution associated with a $3d^9$ admixture in the ground state [43]. If we discount the excitonic contribution in $CeCuAs_2$, which is reasonable since it is not a large gap insulator like Cu_2O, the spectrum resembles the spectra of nominally monovalent copper compounds [43,44] with the XAS excitation effectively corresponding to transitions of the type $2p^6 3d^{10} \rightarrow 2p^5 3d^{10} 4s^1$.

In Fig. 4, we plot the Cu $2p$-$3d$ resonant photoemission spectra over a wide energy range, from E_F to a binding energy of 30 eV, along with an inset which plots a narrow range for the main valence band up to 10 eV binding energy on an expanded intensity (y) scale. The inset shows the main valence band measured with photon energies across the $2p$-$3d$ threshold, labeled a–e in Fig. 3(b). The spectra are normalized to incident photon flux and scan time. Compared to the off-resonance spectrum obtained with energy "a" ($h\nu = 922.7$ eV, same as discussed in Fig. 2), the spectra measured with energies "b" to "e" show a small reduction in intensity of the Cu $3d$ states occurring between 3–5 eV binding energy. In contrast, the spectra plotted in the main panel over a large energy range show a giant resonance at an incident photon energy "c" ($h\nu = 934.6$ eV), corresponding to the peak in the Cu L_3 edge. The giant resonance is well known in CuO, Cu_2O, and the Bi2212 high-temperature copper-oxide superconductor [44]. It occurs due to interference between the direct photoemission channel and the LVV Auger channel for the d^{10} initial state and results in a d^8 final state. The high binding energy three-peak structure actually consists of the atomiclike ^1S, ^1G, and ^3F final-state term splittings of the Cu $3d^8$ configuration [45]. In fact, spin-resolved studies [46] have nicely shown that the highest intensity peak is the ^1G singlet state, the weakest peak at higher binding energy is the ^1S singlet, and the intermediate intensity peak at lower binding energy is the ^3F triplet. While the absolute binding energies of the three-peak structure differ for CuO, Cu_2O, and Bi2212, the energy separations and the

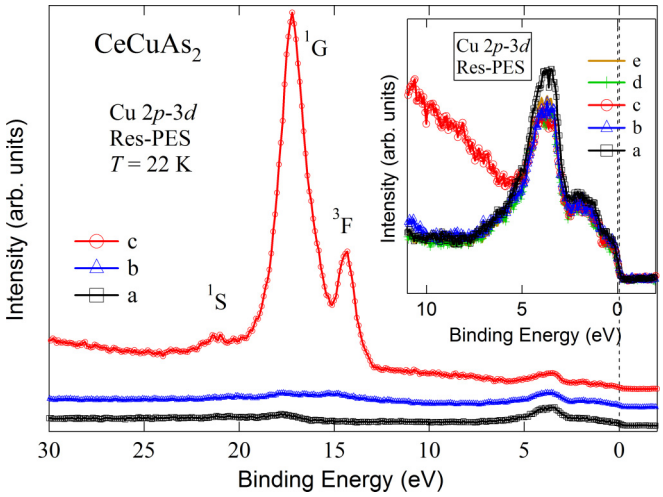

FIG. 4. (Color online) The giant resonance of the satellite seen in the Cu $2p$-$3d$ resonant PES positioned at ~17 eV binding energy, obtained using photon energy $c = 934.6$ eV. The off-resonance spectrum at photon energy $a = 922.7$ eV, and the spectrum obtained at energy $b = 931.6$ eV are also shown for comparison, plotted with a constant shift in intensity. The inset shows a narrower energy range spectra for photon energies a–e [marked in Fig. 3(b)], plotted without any intensity shift but with a magnified intensity scale, in order to show the small changes in the intensity of the Cu $3d$ states in the main valence band.

relative intensities for the constituent peaks are the same as for Cu metal [45] and they also match nicely with our measurements. By analogy, we assign the 17.2- and 21.3-eV peaks to the ^1G and ^1S singlet states while the 14.4-eV peak is assigned to the ^3F triplet state.

We next discuss the Ce $3d$-$4f$ (M-edge) XAS of $CeCuAs_2$ measured at $T = 22$ K and shown in Fig. 5 using symbols. XAS has been extensively used to study Kondo systems in combination with the single-impurity Anderson model [31,32,34–38]. Recent studies have shown that even the

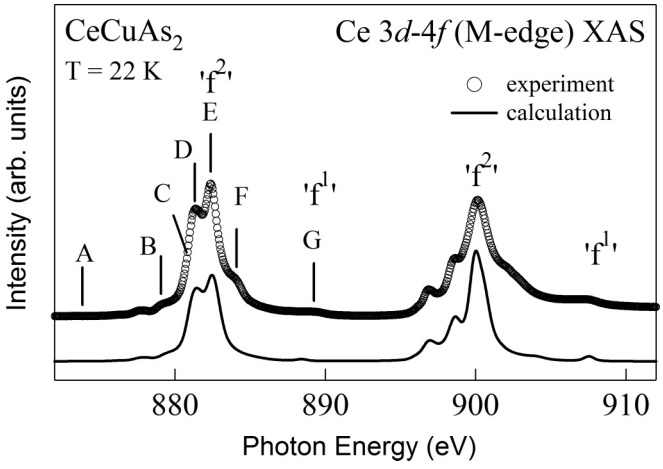

FIG. 5. The Ce $3d$-$4f$ (M-edge) x-ray absorption experimental spectrum (symbols) of $CeCuAs_2$ compared with single-impurity Anderson model calculations (line). Photon energies labeled A–G were used for measuring the Ce $3d$-$4f$ resonant PES spectra.

crystal-field ground states of Ce- and Yb-based rare-earth systems can be very precisely determined using polarization-dependent XAS and ionic full-multiplet model calculations [47]. Here, we follow the first method, pioneered by Gunnarsson-Schonhammer [31] and Fuggle *et al.* [32] in which the single-impurity Anderson model is used to simulate the f^1 and f^2 final states seen in the XAS of Kondo systems. The XAS spectrum of $CeCuAs_2$ shows a very rich structure for the M_5 and M_4 edges (Fig. 5). The calculated XAS spectrum using the single-impurity Anderson model is also shown in Fig. 5 as a line spectrum. The calculated spectrum was obtained using the same set of parameters that were used to calculate the Ce $3d$ core-level HAXPES spectrum shown in Fig. 1. In fact, the parameters were chosen to give the best match to both the core-level HAXPES and the XAS spectra. The main peaks are assigned to the f^2 final state, but we also see a weak but definite feature for the f^1 final states occurring at 889 eV for the M_5 edge and at 907.4 eV for the M_4 edge. The observation of the f^1 final states is a signature of Kondo screening in the final states of XAS [31,32,34–38]. Hence, from the XAS and the core-level HAXPES, the results establish direct evidence for Kondo screening in $CeCuAs_2$. We have then carried out resonant PES across the Ce $3d$-$4f$ threshold at photon energies labeled A–G in Fig. 5. Soft x-ray resonant PES across the $3d$-$4f$ is a powerful method to clarify the $4f$ character partial density of states (DOS) in rare-earth-based materials [48–50]. The Ce $3d$-$4f$ resonant PES spectra measured at $T = 22$ K are shown in Fig. 6. The off-resonant spectrum measured with photon energy A ($h\nu = 873.8$ eV) is quite similar to the spectrum measured with $h\nu = 922.7$ eV (soft x-ray spectrum shown in Fig. 2). As we increase the photon energy, we see a systematic enhancement of the spectral intensity between E_F and about 3 eV binding energy up to the photon energy E, and then the intensity drops down for photon energies F and G. The spectra show a sharp peak near E_F which shows an intense maximum at photon energy E ($h\nu = 882.4$ eV) corresponding to the highest intensity peak in the M_5 edge, and a weak structure at about 2.5 eV binding energy. The peak near E_F is the f^1 final state reflecting

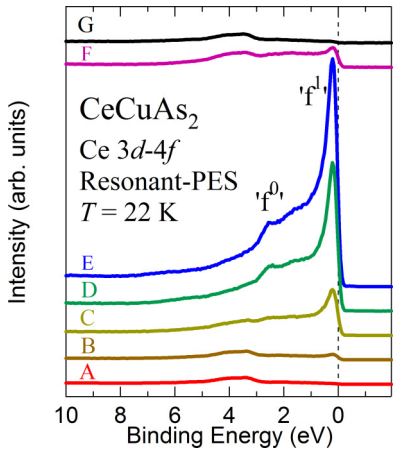

FIG. 6. (Color online) (Color online)) Ce $3d$-$4f$ resonant PES of $CeCuAs_2$ for energies labeled A–E and marked in Fig. 5. The results show a systematic increase in the f partial density of states with an intense resonance maximum for incident photon energy E.

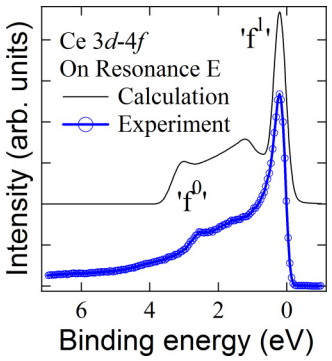

FIG. 7. (Color online) Comparison of experimental results with single-impurity Anderson model calculations for Ce $3d$-$4f$ resonant PES spectrum E. The comparison shows a good match between experiment and calculations carried out using the same parameters as for the Ce $3d$ core level (Fig. 1) and Ce M-edge XAS (Fig. 5).

the Kondo or Abrikosov-Suhl resonance in the valence band, while the peak at 2.5 eV binding energy is the f^0 final state [31–38].

Using the single-impurity Anderson model, we have calculated the Kondo resonance f^1 and the direct photoemission f^0 signal and the results are shown in Fig. 7 compared to the spectrum obtained with photon energy E. Here again, we have used the same parameters as for the Ce $3d$ core-level HAXPES and the M-edge XAS. The calculated result indicates a fairly good match with the experimental spectrum thereby confirming the validity of the Kondo picture. It is noted that for typical low- and high-T_K Kondo metals, the tail of the Kondo resonance is observed as a sharp peak at E_F in the occupied DOS as measured by high-resolution photoemission spectroscopy [51–53]. However, a careful look at the experimental spectrum E as shown on an expanded scale in Fig. 8(a) reveals that the leading edge is not at E_F but just below E_F, and is discussed in detail in the following.

Figure 8(a) shows a comparison of the on-resonance spectrum E with the Fermi-Dirac (FD) function convoluted with a Gaussian function of 200 meV FWHM, corresponding to the energy resolution obtained by fitting to the experimental gold Fermi edge. While our energy resolution is not very high as we are doing a Ce $3d$-$4f$ experiment at about 880 eV incident photon energy to characterize the f partial DOS, a small but finite difference is observed in the leading edge of spectrum E compared to the FD function convoluted with the Gaussian function. In order to obtain the f partial density of states at and near E_F, we have then divided the on-resonance spectrum E by the FD function at $T = 22$ K convoluted by the resolution broadened Gaussian function, and the result is superimposed on the data in Fig. 8(a). The results indicate that the main peak of the occupied f partial density of states is positioned at $\sim 180 \pm 20$ meV below E_F, and shows a dip feature at E_F. In order to further confirm that the dip feature is genuinely of $4f$ character, we have also done a similar exercise with the spectra obtained with photon energies A to F and plotted in Fig. 8(b). Figure 8(b) shows that the dip at E_F evolves systematically with the resonance behavior in

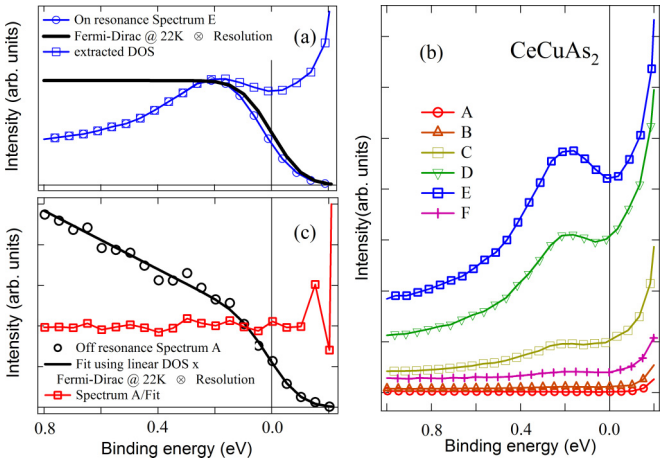

FIG. 8. (Color online) (a) The near E_F on-resonant spectrum E divided by the Fermi-Dirac function at $T = 22$ K convoluted with a Gaussian function corresponding to the experimental energy resolution of 200 meV. The extracted f partial density of states shows a dip at E_F. (b) A similar analysis for the spectra A to F shows the systematic evolution of the dip feature at E_F. (c) In contrast, the off-resonant spectrum A shows a typical metallic Fermi edge. A linear DOS multiplied by the Fermi-Dirac function and convoluted with the experimental Gaussian was used to fit the off-resonant spectrum A.

the partial f DOS and is clear for photon energies D and E, and then gets weakened for spectrum F. On the other hand, the near E_F region of the off-resonance spectrum A [Fig. 8(c)] shows a typical Fermi edge. Here, we needed to use a simple linear DOS multiplied by the FD function at $T = 22$ K convoluted with the same Gaussian function to simulate the off-resonance spectrum A. The spectrum A divided by the fit shows a flat behavior at and near E_F and confirms that the off-resonance spectrum A of $CeCuAs_2$ exhibits a typical metallic Fermi edge. The results indicate that the dip feature is observed only for the f partial DOS which rides on the metallic conduction band DOS. Also, as is well known [54], since the division of the raw spectra by the FD function convoluted Gaussian function is considered valid only up to an energy of $\sim 4k_BT$ above E_F, i.e., ~ 10 meV at $T = 22$ K, we clarify that the dip feature is effectively identified from the f partial DOS at and just below E_F, and which reflects the difference compared to the metallic Fermi edge. It would be thus useful to carry out temperature-dependent studies of the f partial DOS, but at a higher-energy resolution. This is possible with Ce $4d$-$4f$ resonant PES [55], but it is expected to be more surface sensitive than the present experiments and is beyond the scope of this study.

Finally, although we see a pseudogap in the f partial DOS at E_F, in order to check whether it is a signature of underscreening in the Kondo model, we have analyzed the magnetic susceptibility $\chi(T)$ of $CeCuAs_2$ by plotting $T\chi(T)$ versus $\ln T$, as discussed in the Appendix. The results show no enhancement of the spin moment below room temperature down to the lowest temperature of measurement ($T = 1.8$ K). Instead, a faster than logarithmic decrease in $T\chi(T)$ is observed on reducing temperature. This rules out an underscreened Kondo effect as discussed by Nevidomskyy and Coleman [17], and is suggestive of antiferromagnetic correlations [18,28] in $CeCuAs_2$. However, the Ce $3d$ core-level HAXPES, Ce M-edge XAS, and the Ce $3d$-$4f$ resonant PES results consistently show evidence for Kondo screening in the spectroscopic properties of $CeCuAs_2$ and a pseudogap in the f partial DOS at E_F. The electronic states at and near E_F would play an important role in the anomalous transport and magnetic properties of $CeCuAs_2$. A recent study on a nonsuperconducting iron-pnictide FeCrAs which shows antiferromagnetic ordering has proposed a non-Fermi-liquid ground state based on a power-law behavior observed in electrical transport properties [56]. It would be important to carry out spectroscopic studies on FeCrAs to check for a pseudogap behavior in another pnictide compound, but in the presence of magnetic ordering.

IV. CONCLUSIONS

In conclusion, we have carried out spectroscopic studies of $CeCuAs_2$ using hard x-ray photoemission spectroscopy (HAXPES), x-ray absorption spectroscopy (XAS), and resonant PES. The Ce $3d$ core-level PES shows typical Kondo behavior in terms of the f^0, f^1, and f^2 features, while the Ce $3d$-$4f$ XAS shows corresponding features due to transitions into the f^1 and f^2 states. The spectral feature assignments are confirmed by single-impurity Anderson model calculations and indicate a nearly trivalent-Ce configuration. The resonant PES valence band spectra across the Cu $2p$-$3d$ threshold show a giant resonance for the high binding energy satellite. The Ce $3d$-$4f$ resonant PES spectra show an intense Ce $4f^1$ resonance just below the Fermi level, with the Ce $4f^0$ feature positioned at a binding energy of 2.5 eV. The obtained f partial density of states shows a pseudogaplike dip at the Fermi level in $CeCuAs_2$. The results indicate Kondo screening and the pseudogap in the f partial density of states lead to the anomalous transport and magnetic properties of $CeCuAs_2$.

ACKNOWLEDGMENTS

We thank Dr. S. Florens, Dr. K. Matho, and Professor H. R. Krishnamurthy for very valuable discussions. The experiments were carried out with the approval of the RIKEN SPring-8 Center (Proposal No. 20100021).

APPENDIX

Analysis of the magnetic susceptibility $\chi(T)$ of $CeCuAs_2$: In a recent theoretical study, Nevidomskyy and Coleman addressed the general behavior of the role of Hund's coupling on the Kondo effect for d and f electron systems [17]. While the Hund's coupling is not important for an f^1 electron system (such as Ce^{3+}) at the single-ion level, it was shown that for a single-site multi(K)-channel Kondo model with Hund's coupling, underscreening leads to a locking of localized spin-$\frac{1}{2}$ moments to form a large pseudospin $S = K/2$. The enhancement in the effective spin moment is accompanied by an exponential reduction of the effective Kondo temperature T_K^*. The underscreening behavior can then

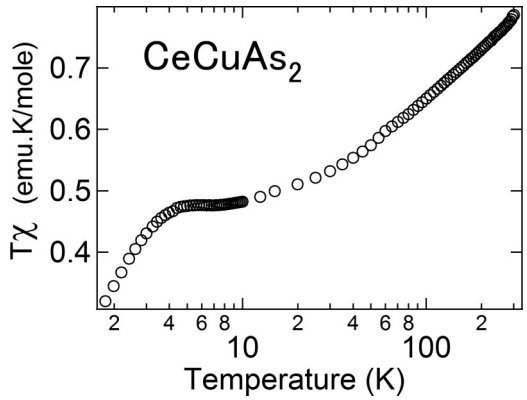

FIG. 9. Plot of $T\chi(T)$ vs $\ln T$ for $CeCuAs_2$, using the $\chi(T)$ reported in Ref. [16]. The plot shows a faster than logarithmic decrease on reducing temperature down to about 10 K. At lower temperatures, a plateau region between 5–10 K is clearly seen, followed by a further reduction below 5 K.

be identified from a plot of $T\chi(T)$ versus $\ln T$, which is expected to show three regions: (i) a high-T paramagnetic phase with spin-$\frac{1}{2}$ moments, (ii) an intermediate-T phase with a large unscreened pseudospin $S = K/2$ at temperatures above T_K^*, and (iii) a low-T Nozieres Fermi liquid ground state below T_K^*. This result provides a good method to test for underscreening and we apply it here for the case of $CeCuAs_2$.

In Fig. 9, we plot $T\chi(T)$ versus $\ln T$ using the magnetic susceptibility data reported earlier for $T = 1.8$–300 K [16]. As is clearly seen in the figure, $T\chi(T)$ shows a faster than logarithmic decay below 300 K, all the way down to about 10 K. This rules out an enhancement of the effective spin moment and is, instead, typical of antiferromagnetic spin correlations [18,28]. The data at low temperatures shows a plateau region between 5–10 K and then a further reduction down to the lowest temperature. The plateau region corresponds to an anomalous plateau also seen in the specific-heat data, and has been discussed earlier [16]. The quenching of the spin moment at the lowest temperatures suggests a very low $T_K^* \ll 1$ K. Thus, in conclusion, $CeCuAs_2$ does not show an enhanced effective spin moment and can not be considered as an example of the underscreened Kondo effect.

[1] J. Kondo, Prog. Theor, Phys. **32**, 37 (1964).
[2] A. C. Hewson, *The Kondo Problem to Heavy Fermions* (Cambridge University Press, Cambridge, 1993).
[3] G. R. Stewart, Rev. Mod. Phys. **56**, 755 (1984).
[4] J. W. Allen and R. M. Martin, Phys. Rev. Lett. **49**, 1106 (1982); M. Lavagna, C. Lacroix, and M. Cyrot, Phys. Lett. A **90**, 210 (1982).
[5] M. A. Reed, J. N. Randall, R. J. Aggarwal, R. J. Matyi, T. M. Moore, and A. E. Wetsel, Phys. Rev. Lett. **60**, 535 (1988); S. M. Cronenwett, T. H. Oosterkamp, and L. P. Kouwenhoven, Science **281**, 540 (1998).
[6] M. F. Crommie, C. P. Lutz, and D. M. Eigler, Science **262**, 218 (1993).
[7] N. Tsukahara, S. Shiraki, S. Itou, N. Ohta, N. Takagi, and M. Kawai, Phys. Rev. Lett. **106**, 187201 (2011).
[8] Q. Si and S. Paschen, Phys. Status Solidi B **250**, 425 (2013).
[9] L. de' Medici, A. Georges, G. Kotliar, and S. Biermann, Phys. Rev. Lett. **95**, 066402 (2005).
[10] A. M. Sengupta and A. Georges, Phys. Rev. B **52**, 10295 (1995).
[11] S. Pankov, S. Florens, A. Georges, G. Kotliar, and S. Sachdev, Phys. Rev. B **69**, 054426 (2004).
[12] P. Coleman and C. Pepin, Phys. Rev. B **68**, 220405 (2003).
[13] S. Florens, Phys. Rev. B **70**, 165112 (2004).
[14] P. Coleman and I. Paul, Phys. Rev. B **71**, 035111 (2005).
[15] C. Thomas, A. S. daRosa Simoes, J. R. Iglesias, C. Lacroix, N. B. Perkins, and B. Coqblin, Phys. Rev. B **83**, 014415 (2011).
[16] K. Sengupta, E. V. Sampathkumaran, T. Nakano, M. Hedo, M. Abliz, N. Fujiwara, Y. Uwatoko, S. Rayaprol, K. Shigetoh, T. Takabatake, Th. Doert, and J. P. F. Jemetio, Phys. Rev. B **70**, 064406 (2004).
[17] A. H. Nevidomskyy and P. Coleman, Phys. Rev. Lett. **103**, 147205 (2009).
[18] C. Jayaprakash, H. R. Krishna-murthy, and J. W. Wilkins, Phys. Rev. Lett. **47**, 737 (1981).
[19] H. Sprenger, J. Less-Common Met. **34**, 39 (1974).
[20] J. Stepien-Damm, D. Kaczorowski, and R. Troc, J. Less-Common Met. **132**, 15 (1987).
[21] M. Brylak, M. H. Moller, and W. Jeitschko, J. Solid State Chem. **115**, 305 (1995).
[22] D. Rutzinger, C. Bartsch, M. Doerr, H. Rosner, V. Neu, Th. Doert, and M. Ruck, J. Solid State Chem. **183**, 510 (2010).
[23] S. Araki, N. Metoki, A. Galatanu, E. Yamamoto, A. Thamizhavel, and Y. Onuki, Phys. Rev. B **68**, 024408 (2003); A. Thamizhavel, T. Takeuchi, T. Okubo, M. Yamada, R. Asai, S. Kirita, A. Galatanu, E. Yamamoto, T. Ebihara, Y. Inada, R. Settai, and Y. Onuki, *ibid.* **68**, 054427 (2003).
[24] E. V. Sampathkumaran, K. Sengupta, S. Rayaprol, K. K. Iyer, Th. Doert and J. P. F. Jemetio, Phys. Rev. Lett. **91**, 036603 (2003); K. Sengupta, S. Rayaprol, E. V. Sampathkumaran, Th. Doert, and J. P. F. Jemetio, Phys. B (Amsterdam) **348**, 465 (2004).
[25] M. Szlawska and D. Kaczorowski, J. Alloys Compd. **451**, 464 (2008).
[26] D. Kaczorowski, R. Kruk, J. P. Sanchez, B. Malaman, and F. Wastin, Phys. Rev. B **58**, 9227 (1998).
[27] M. Abliz, T. Nakano, E. V. Sampathkumaran, J. P. F. Jemetio, Th. Doert, M. Hedo, and Y. Uwatoko, J. Phys. Soc. Jpn. **74**, 508 (2005).
[28] S. J. Blundell, *Magnetism in Condensed Matter* (Oxford University Press, Oxford, 2001), p. 93.
[29] Y. Takata, M. Yabashi, K. Tamasaku, Y. Nishino, D. Miwa, T. Ishikawa, E. Ikenaga, K. Horiba, S. Shin, M. Arita, K. Shimada, H. Namatame, M. Taniguchi, H. Nohira, T. Hattori,

S. Sodergren, B. Wannberg, and K. Kobayashi, Nucl. Instrum. Methods Phys. Res., Sect. A **547**, 50 (2005); T. Ishikawa, K. Tamasaku, and M. Yabashi, *ibid.* **547**, 42 (2005).

[30] K. Horiba, N. Kamakura, K. Yamamoto, K. Kobayashi, and S. Shin, J. Electron Spectrosc. Relat. Phenom. **144**, 1027 (2005).

[31] O. Gunnarsson and K. Schonhammer, Phys. Rev. Lett. **50**, 604 (1983); Phys. Rev. B **28**, 4315 (1983).

[32] J. C. Fuggle, F. U. Hillebrecht, J.-M. Esteva, R. C. Karnatak, O. Gunnarsson, and K. Schonhammer, Phys. Rev. B **27**, 4637 (1983).

[33] E. Wuilloud, H. R. Moser, W.-D. Schneider, and Y. Baer, Phys. Rev. B **28**, 7354 (1983).

[34] J. W. Allen, J. Phys. Soc. Jpn. **74**, 34 (2005).

[35] L. Z. Liu, J. W. Allen, O. Gunnarsson, N. E. Christensen, and O. K. Andersen, Phys. Rev. B **45**, 8934 (1992).

[36] Yu. Kucherenko, S. L. Molodtsov, M. Heber, and C. Laubschat, Phys. Rev. B **66**, 155116 (2002).

[37] C. Dallera, M. Grioni, A. Palenzona, M. Taguchi, E. Annese, G. Ghiringhelli, A. Tagliaferri, N. B. Brookes, Th. Neisius, and L. Braicovich, Phys. Rev. B **70**, 085112 (2004).

[38] M. Matsunami, K. Horiba, M. Taguchi, K. Yamamoto, A. Chainani, Y. Takata, Y. Senba, H. Ohashi, M. Yabashi, K. Tamasaku, Y. Nishino, D. Miwa, T. Ishikawa, E. Ikenaga, K. Kobayashi, H. Sugawara, H. Sato, H. Harima, and S. Shin, Phys. Rev. B **77**, 165126 (2008).

[39] T. Tolinski, A. Kowalczyk, G. Chelkowska, M. Pugaczowa-Michalska, B. Andrzejewski, V. Ivanov, A. Szewczyk, and M. Gutowska, Phys. Rev. B **70**, 064413 (2004).

[40] J. J. Yeh and I. Lindau, At. Data Nucl. Data Tables **32**, 1 (1985).

[41] S. de Jong, Y. Huang, R. Huisman, F. Massee, S. Thirupathaiah, M. Gorgoi, F. Schaefers, R. Follath, J. B. Goedkoop, and M. S. Golden, Phys. Rev. B **79**, 115125 (2009).

[42] J. Ghijsen, L. H. Tjeng, J. van Elp, H. Eskes, J. Westerink, G. A. Sawatzky, and M. T. Czyzyk, Phys. Rev. B **38**, 11322 (1988), and references therein.

[43] M. Grioni, J. B. Goedkoop, R. Schoorl, F. M. F. de Groot, J. C. Fuggle, F. Schafers, E. E. Koch, G. Rossi, J.-M. Esteva, and R. C. Karnatak, Phys. Rev. B **39**, 1541 (1989); M. Grioni, J. F. van Acker, M. T. Czyzyk, and J. C. Fuggle, *ibid.* **45**, 3309 (1992).

[44] L. H. Tjeng, C. T. Chen, J. Ghijsen, P. Rudolf, and F. Sette, Phys. Rev. Lett. **67**, 501 (1991); L. H. Tjeng, C. T. Chen, and S-W. Cheong, Phys. Rev. B **45**, 8205 (1992).

[45] E. Antonides, E. C. Janse, and G. A. Sawatzky, Phys. Rev. B **15**, 1669 (1977).

[46] L. H. Tjeng, B. Sinkovic, N. B. Brookes, J. B. Goedkoop, R. Hesper, E. Pellegrin, F. M. F. de Groot, S. Altieri, S. L. Hulbert, E. Shekel, and G. A. Sawatzky, Phys. Rev. Lett. **78**, 1126 (1997); N. B. Brookes, G. Ghiringhelli, O. Tjernberg, L. H. Tjeng, T. Mizokawa, T. W. Li, and A. A. Menovsky, *ibid.* **87**, 237003 (2001).

[47] P. Hansmann, A. Severing, Z. Hu, M. W. Haverkort, C. F. Chang, S. Klein, A. Tanaka, H. H. Hsieh, H.-J. Lin, C. T. Chen, B. Fak, P. Lejay, and L. H. Tjeng, Phys. Rev. Lett. **100**, 066405 (2008); T. Willers, J. C. Cezar, N. B. Brookes, Z. Hu, F. Strigari, P. Korner, N. Hollmann, D. Schmitz, A. Bianchi, Z. Fisk, A. Tanaka, L. H. Tjeng, and A. Severing, *ibid.* **107**, 236402 (2011); F. Strigari, T. Willers, Y. Muro, K. Yutani, T. Takabatake, Z. Hu, S. Agrestini, C.-Y. Kuo, Y.-Y. Chin, H.-J. Lin, T. W. Pi, C. T. Chen, E. Weschke, E. Schierle, A. Tanaka, M. W. Haverkort, L. H. Tjeng, and A. Severing, Phys. Rev. B **87**, 125119 (2013).

[48] A. Sekiyama, T. Iwasaki, K. Matsuda, Y. Saitoh, Y. Onuki, and S. Suga, Nature (London) **403**, 396 (2000).

[49] E. J. Cho, R. J. Jung, B. H. Choi, S. J. Oh, T. Iwasaki, A. Sekiyama, S. Imada, S. Suga, T. Muro, J. G. Park, and Y. S. Kwon, Phys. Rev. B **67**, 155107 (2003).

[50] M. Matsunami, R. Eguchi, T. Kiss, K. Horiba, A. Chainani, M. Taguchi, K. Yamamoto, T. Togashi, S. Watanabe, X.-Y. Wang, C.-T. Chen, Y. Senba, H. Ohashi, H. Sugawara, H. Sato, H. Harima, and S. Shin, Phys. Rev. Lett. **102**, 036403 (2009); M. Matsunami, M. Taguchi, A. Chainani, R. Eguchi, M. Oura, A. Sakai, S. Nakatsuji, and S. Shin, Phys. Rev. B **84**, 193101 (2011).

[51] D. Malterre, M. Grioni, and Y. Baer, Adv. Phys. **45**, 299 (1996).

[52] M. Garnier, K. Breuer, D. Purdie, M. Hengsberger, Y. Baer, and B. Delley, Phys. Rev. Lett. **78**, 4127 (1997).

[53] F. Reinert, D. Ehm, S. Schmidt, G. Nicolay, S. Hufner, J. Kroha, O. Trovarelli, and C. Geibel, Phys. Rev. Lett. **87**, 106401 (2001); D. Ehm, S. Hufner, F. Reinert, J. Kroha, P. Wolfle, O. Stockert, C. Geibel, and H. v. Lohneysen, Phys. Rev. B **76**, 045117 (2007).

[54] T. Greber, T. J. Kreutz, and J. Osterwalder, Phys. Rev. Lett. **79**, 4465 (1997).

[55] K. Shimada, K. Kobayashi, T. Narimura, P. Baltzer, H. Namatame, M. Taniguchi, T. Suemitsu, T. Sasakawa, and T. Takabatake, Phys. Rev. B **66**, 155202 (2002).

[56] W. Wu, A. McCollam, I. Swainson, P. M. C. Rourke, D. G. Rancourt, and S. R. Julian, Europhys. Lett. **85**, 17009 (2009).